










A Wearable Device Towards Automatic Detection and Treatment of Opioid Overdose

Juan C. Mesa , Michael D. MacLean , María MS , Alan Nguyen , Rujuta Patel , Timothy Diemer , Jongcheon Lim , Chi Hwan Lee , and Hyowon Lee , *Member, IEEE*

Abstract—Opioid-induced overdose is one of the leading causes of death among the US population under the age of 50. In 2021 alone, the death toll among opioid users rose to a devastating number of over 80,000. The overdose process can be reversed by the administration of naloxone, an opioid antagonist that rapidly counteracts the effects of opioid-induced respiratory depression. The idea of a closed-loop opioid overdose detection and naloxone delivery has emerged as a potential engineered solution to mitigate the deadly effects of the opioid epidemic. In this work, we introduce a wrist-worn wearable device that overcomes the portability issues of our previous work to create a closed-loop drug-delivery system, which includes (1) a Near-Infrared Spectroscopy (NIRS) sensor to detect a hypoxia-driven opioid overdose event, (2) a MOSFET switch, and (3) a Zero-Voltage Switching (ZVS) electromagnetic heater. Using brachial artery occlusion (BAO) with human subjects ($n = 8$), we demonstrated consistent low oxygenation events. Furthermore, we proved our device's capability to release the drug within 10 s after detecting a hypoxic event. We found that the changes in the oxyhemoglobin, deoxyhemoglobin and oxygenation saturation levels (SpO_2) were different before and after the low-oxygenation events ($p < 0.001$). Although additional human experiments are needed, our results to date point towards a potential tool in the battle to mitigate the effects of the opioid epidemic.

Index Terms—Opioid overdose, closed-loop wearable devices, near-infrared spectroscopy (NIRS), oxygen saturation (SpO_2), naloxone, respiratory depression.

I. INTRODUCTION

OPIOID-RELATED deaths in the United States (US) rose to 49,860 in 2019, followed by another sharp increase over 80,000 approximately in 2021 representing more than 75% of the total national drug overdose deaths [1], [2]. Over 87% of these deaths involve fast-acting synthetic opioids such as fentanyl, which can significantly increase the risk of mortality due to its extremely high potency [2]. Physicians use opioids for pain management, especially for those patients suffering from severe illnesses [3], [4], [5]. However, the misuse of opioids roughly affects vital physiological processes in the central nervous system, leading to devastating hypoxic events and severe cardiorespiratory depression [5], [6], [7], [8].

The current method to address an opioid overdose is to administer a burst dose of naloxone, a Federal Drug Administration (FDA) approved strong opiate antagonist that counteracts the physiological effects of an opioid-induced cardiorespiratory depression event [9], [10]. Naloxone is an indispensable harm reduction tool in the battle against the ongoing opioid epidemic [11]. Most commonly, naloxone has been shown to be effective when administered via nasal inhalation, intramuscular or subcutaneous injections [9], [12].

To reverse the life-threatening effects of an opioid overdose, it is crucial to deliver the antidote as fast as possible [13], [14]. However, opioid users are often found unconscious with limited capability to properly self-administrate the life-saving medicine. Therefore, there is a critical need to develop a system that can rapidly detect an opioid-induced respiratory depression and deliver a burst amount of naloxone automatically, especially for patients residing in rural areas and places with limited access to healthcare systems.

The development of wearable devices for the detection of opioid overdose and naloxone drug delivery is one of the most promising harm-reduction technologies to address the mortality associated with the opioid epidemic. The Q sensor was the first wrist-wearable system capable of measuring physiological changes including skin electrodermal activity (EDA), skin temperature, and 3D locomotion to establish correlations with an opioid-overdose event. However, further studies proved that EDA and locomotion were not strongly statistically valid

Manuscript received 17 June 2023; revised 22 August 2023 and 27 October 2023; accepted 31 October 2023. Date of publication 8 November 2023; date of current version 29 March 2024. This paper was recommended by Associate Editor S. Ghoreishizadeh. (Juan C. Mesa and Michael D. MacLean are co-first authors.) (Corresponding author: Hyowon Lee.)

This work involved human subjects or animals in its research. Approval of all ethical and experimental procedures and protocols was granted by the Purdue Human Research Protection Program and Institutional Review Board under Application No. Protocol IRB-2020-297.

Juan C. Mesa, Michael D. MacLean, María MS, Alan Nguyen, Rujuta Patel, Jongcheon Lim, and Hyowon Lee are with the Weldon School of Biomedical Engineering, Purdue University, West Lafayette, IN 47907 USA, also with the Center for Implantable Devices, Purdue University, West Lafayette, IN 47907 USA, and also with the Birck Nanotechnology Center, Purdue University, West Lafayette, IN 47907 USA (e-mail: jmesaagu@purdue.edu; mmaclea@purdue.edu; molinasa@purdue.edu; nguy372@purdue.edu; patel840@purdue.edu; lim263@purdue.edu; hwlee@purdue.edu).

Timothy Diemer is with the Center for Implantable Devices, Purdue University, West Lafayette, IN 47907 USA, also with the Birck Nanotechnology Center, Purdue University, West Lafayette, IN 47907 USA, and also with the Emory Family School of Electrical Engineering, Purdue University, West Lafayette, IN 47907 USA (e-mail: diemert@purdue.edu).

Chi Hwan Lee is with the Weldon School of Biomedical Engineering, Purdue University, West Lafayette, IN 47907 USA, also with the Center for Implantable Devices, Purdue University, West Lafayette, IN 47907 USA, also with the Birck Nanotechnology Center, Purdue University, West Lafayette, IN 47907 USA, also with the School of Materials Engineering, Purdue University, West Lafayette, IN 47907 USA, and also with the School of Mechanical Engineering, Purdue University, West Lafayette, IN 47907 USA (e-mail: lee2270@purdue.edu).

Color versions of one or more figures in this article are available at <https://doi.org/10.1109/TBCAS.2023.3331272>.

Digital Object Identifier 10.1109/TBCAS.2023.3331272

to confirm correlations with an opioid-related drug overdose event [15].

Recently, a team of engineers and clinicians developed a closed-loop proof-of-concept wearable injector system of naloxone. The wearable system measures opioid-induced apnea events and respiratory depression, implementing a pair of body accelerometers and administering naloxone through a commercial injector system [16]. This wearable technology was tested in two controlled scenarios: (i) a certified injection facility where patients self-administered a predetermined opioid dose, and (ii) a simulated hospital setting created to mimic an opioid-related event. Although the authors demonstrated the device's capability to successfully detect apnea events related to an opioid-overdose, the system is relatively bulky and easily perceivable through the garments as designed. Additionally, the invasiveness of having an injector system could potentially increase the risk of infections, diminish the willingness of patients to use the device due to needle phobia, and other side effects.

The system detailed in this work relies on optical sensors to detect opioid-induced apnea and respiratory depression events, based on blood oxygenation levels. Photoplethysmography (PPG) is a widely used noninvasive technique that measures oxygenation levels and collects electrocardiographic information by utilizing the absorbance property of oxygenated and deoxygenated hemoglobin. PPG implements a light transmitter to propagate through the tissue and a photodetector to perceive the changes in the emitted light at different wavelengths [17]. Using PPG, researchers were able to accurately detect 90% of opioid-induced cardiorespiratory events [18]. Empatica E4, a wrist-mounted PPG biosensor was implemented for the detection and recovery process of opioid-related overdose use [19], [20]. Recently, a team of engineers developed a proof-of-concept wearable hypoxia-driven device for opioid-overdose response [21]. The wearable system utilizes a PPG-based oximeter to detect an opioid-overdose, a GPS tracker to alert 911 of the overdose events, and an injection system based on a plunger, compressed gas and a commercial needle to deliver naloxone. However, this wearable system was not tested in an overdose-simulated environment and the performance of the injector was only evaluated in silico.

In this work, we used a subset of PPG, near-infrared spectroscopy (NIRS), which is an optical technique that can detect the cardiopulmonary activity of the body using red and infrared (IR) light-emitting diodes (LEDs) [17]. NIRS is a well-known technique to non-invasively assess oxygenation and blood volumes that utilizes conventional circuits and instrumentation. This technique relies on the capacity of IR light to penetrate deep into living tissues due to low absorption and high scattering properties, revealing proportional attenuation of the light to the specific changes in the concentration of chromophores in the tissue [17], [22]. Using the relationship with the absorbance of oxyhemoglobin (HbO_2) and deoxyhemoglobin (HbR), it is possible to estimate a crucial parameter notated as the modulation index (R) to determine the (SpO_2) levels through a calibration curve [23], [24], [25], [26], [27]. Healthy subjects have SpO_2 levels between 95 – 100%, but it could slightly vary depending on the cardiorespiratory conditions of the

patients. Some individuals with lung abnormalities oxygenate at lower levels, which indicates an irregular perfusion-oxygenated event on the subject's blood [28]. The SpO_2 values $< 90\%$ could serve as an indicator of an opioid-overdose and hypoxia event, revealing the need of urgent care as soon as possible [21].

Herein, we present the development of a wrist-wearable prototype with closed-loop to detect opioid-induced cardiorespiratory depression to deliver a burst of naloxone validated with human experiments under brachial artery occlusion (BAO) events. The system emerges as an improvement of our previous work [29], implementing a fully wearable device based on NIRS, overcoming the limitations of portability of the aforementioned device. The wearable system consists of three main stages. (i) A sensor based on NIRS technology to detect cardiopulmonary depression based on hypoxia events; (ii) a MOSFET switch to activate the actuator; (iii) an modified electromagnetic field generator based on the Zero Voltage Switching (ZVS) circuit to deliver the live-saving antidote as quickly as possible.

II. METHODS

A. Design and Fabrication

Fig. 1 shows the design of the main stages of the wearable device. This device consists of three main electronic systems; a NIRS sensor (Fig. 1(a)), a MOSFET switch (Fig. 1(b)), and an electromagnetic ZVS actuator (Fig. 1(c)).

1) *Sensor NIRS*: Figs. 1(a) illustrate the electronic components involved in the design of the NIRS sensor. The SFH7050 (OS-RAM Opto Semiconductors, Regensburg, Germany) represents the optical source of the sensor, which contains three LEDs with specific wavelengths $\lambda = 525$ nm (green), $\lambda = 660$ nm (red), $\lambda = 950$ nm (IR) and a photodiode, used to serve as the light source of the device (see Fig. 2(b) for more details). Each LED was pulsed out of phase at a frequency of 14.05 Hz, establishing an on-time pulse of 15 ms to yield a duty cycle of 0.21. We conditioned the output from the optical sensor using a transimpedance amplifier (TIA), based on a conventional design along with a low-pass filter, an analog-to-digital converter (ADC), a voltage regulator, and miscellaneous sub-circuits to guarantee a suitable operation of the system. To handle the logic of the system, we used an open-source microcontroller (SAM21G18AU, Microchip Technology, Inc, Chandler, AZ, USA).

2) *LED Driver*: In order to meet the power consumption requirements of the optical source within the system and to enable light measurement from the detection side, we designed an LED driver using a configuration of MOSFETs and resistors (see Fig. 2(b)). We implemented a current-limiting resistor to control the current and connect the system to ground. To determine the maximum current ratings for each color channel, we calculated the resistance values and manually adjusted the resistors to achieve a similar photocurrent output at the photodiode (see Fig. 2(b)). The resistor selection took into account the pulse current requirements of the SFH7050 LED for the three channels, as specified in its datasheet [30]. Considering current pulses of 100 mA (IR LED), 66 mA (Red LED), and 45 mA (Green LED), along with the voltage drops across these

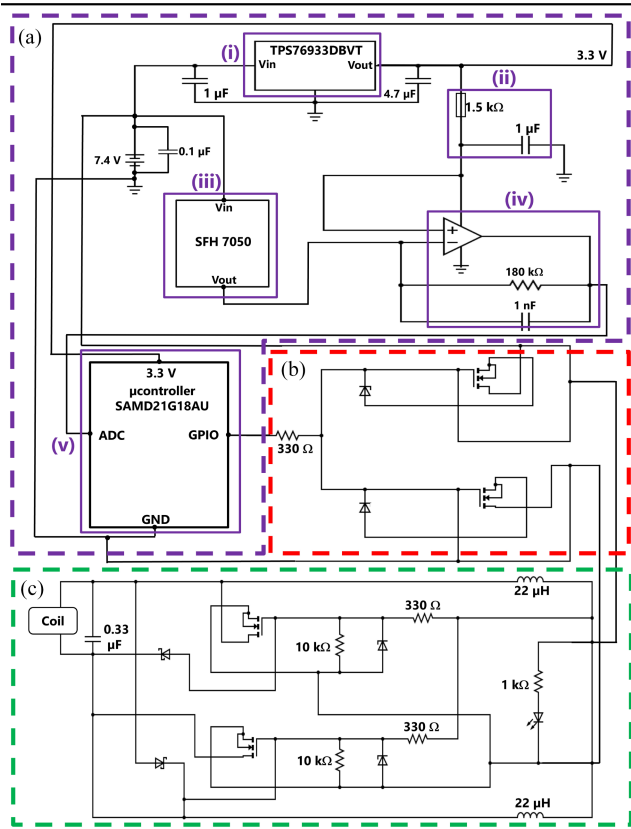


Fig. 1. Electronic design of the drug delivery system. (a) Block diagram of the principal electronic elements of the NIRS sensor; (i) The 3.3 V supply from the voltage regulator; (ii) the ferrite bead and decoupling capacitor to stabilize the power supply signal; (iii) the photodiode from the SFH7050 and the power supply (lithium batteries); (iv) configuration of the TIA along with a low-pass filter to smooth the signal and; (v) the microcontroller of the system (SAMD21G18AU). (b) Block diagram of the Dual MOSFET trigger switch. (c) Block diagram of the ZVS electromagnetic field generator.

diodes and their internal resistances, we calculated the current-limiting resistor using (1). Subsequently, we set the output for each channel color to the same bit value to prevent issues of over-and under-saturation. Fig. 2(d) depicts a representation of LED wavelengths penetrating the skin tissue to assess changes in absorbance within the capillaries.

$$R_{limit} = V_{supp}/I - R_{LED} \quad (1)$$

3) *Transimpedance Amplifier Circuit (TIA)*: To convert the light changes from the photodiode into readable voltage values for the ADC, we implemented a TIA (Figs. 1(a)). We used a simple design with four main components: a low-noise and low quiescent current, precision operational amplifier (OPA376, Texas Instruments, Inc, Dallas, TX, USA), a combination of gain-setting resistors, a feedback capacitor, and a ferrite bead. We reversed the light source of the system (the photodiode) biased by 4.1 V based on the power drop due to the interaction between the two system batteries (7.4 V) and a voltage regulator (3.3 V). We placed the anode from the photodiode at the input of the TIA to ensure a current flow from the photocurrent toward the main circuit. We used a large feedback resistor ($R = 180 \text{ k}\Omega$)

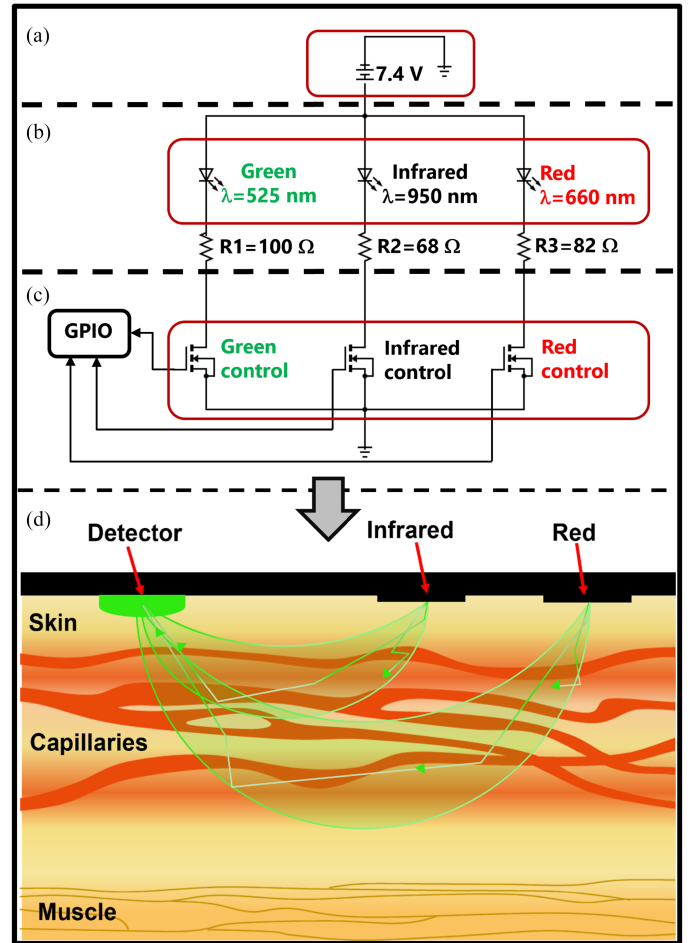


Fig. 2. LED driver circuit with MOSFETS and resistors. (a) The power supply of 2 lithium batteries in series (7.4 V). (b) 3 LEDs of different colors for the NIRS approach. (c) Control signals handled by the microcontroller. (d) Representation of LEDs wavelengths penetration over the skin tissue to evaluate the changes in absorbance on the capillaries.

to obtain readable voltages, considering current values of $1 \mu\text{A}$, the output of the TIA displays values greater than 0.18 V .

To smooth the output signal and attenuate high frequency jitters, we implemented an RC low-pass filter integrated to the TIA with a cutoff frequency of 885 Hz by connecting a capacitor ($C = 1 \text{ nF}$) in parallel with the feedback resistor ($R = 180 \text{ k}\Omega$). This configuration provided stability to the analog system, resulting in a desirable transimpedance gain of approximately 100 (V/A) dB as specified in the OPA376 datasheet [31]. In terms of the cutoff frequency design of the low-pass circuit, we designed the system only to attenuate those signals above the spectra of interest, which is further adjusted by digital filtering processing. Although human NIRS signals do not have a considerable spectrum above 10 Hz, our system operates in pulse mode, requiring pulses of 15 ms, without losing significant data within the spectra of interest. Finally, to enhance the stability of the system, we implemented a bypass capacitor ($C = 1 \mu\text{F}$) and a $1.5 \text{ k}\Omega$ ferrite bead to decouple the power supply signal.

4) *Switch*: To properly pair the sensing and instrumentation circuit (low-current system) and meet the actuator power requirements (electromagnetic field generator), we used a commercial dual high-power SWITCH (dual MOSFET Tigger Switch 0–20 kHz PMW, Amazon.com, Inc). We connected the switch to the ZVS circuit through the microcontroller as illustrated in Fig. 1(b).

5) *ZVS Module*: We modified a compact version of a commercial ZVS (Yooso ZVS Driver Circuit, Amazon.com, Inc), based on the driver electromagnetic field generator implemented in our previous work [29]. To reduce the size of the device as much as possible, we implemented small choke inductors, which are commonly used to block high-frequency voltage signals. At the same time, this family of inductors allows direct current (DC) and low alternative frequencies (AC) to pass while maintaining the properties of the original signal. Fig. 1(c) shows the electronic circuit of the modified ZVS driver. The PCB was designed with a license specialized program (Altium, San Diego, CA, USA) and manufactured by (JLPCB, Inc). To improve the ZVS performance in terms of heat transfer, we constructed a 9 turns pancake copper coil, using a commercial polyamide-insulated magnetic wire (Magnet Wire MW35-C HY). We measured the inductance of the package coil using a commercial LCR meter (LCR meter IM3535, Hioki, Inc, Dallas, TX, USA).

B. Wrist Design and Electronic Housing

To ensure proper isolation between the three main electronic components of the system and avoid undesirable short circuits within the case, we placed a 1 mm layer of Ecoflex 00-30 over the top surface of the circuits. Further, we packed the elements inside the wrist case to be used for the benchtop experiments.

1) *Digital Data Acquisition*: We acquired the sample data considering the 14.05 Hz sampling rate of the LEDs using the microcontroller and the ADC converter (ADS115 16-bit resolution, Texas Instruments, Inc, Dallas, TX, USA). We only used 15 bits of the system due to a slight drop in the negative values of the signal, resulting in a minor modification of 0.1 mV resolution on a 3.3 V instrumentation-powered system. We saved the acquired data as a text file for further processing in Python.

2) *Digital Filtering*: Due to the limitation of current analog circuits to filter data from NIRS devices concerning low peripheral oxygenation applications, we acquired the raw data from the wearable device and further digitally processed on a computer. We applied three principal filters as follows. First, we implemented a fifth order finite impulse response (FIR) low pass to smooth the raw data. We configured this filter for a $f_{stop} = 2.0$ Hz and $f_{pass} = 1.5$ Hz (least squares) with equally weighted passband and stopband. Second, we used a third order infinite impulse response (IIR) Butterworth filter with a cutoff frequency (f_c) of 0.25 Hz to eliminate the low frequency movement effects and the DC offset. Further, we extracted and placed into an array the peak-to-peak voltages values for a 40-sample epoch. Finally, we applied a five-sample sliding median filter to smooth the final signal in terms of further fluctuations caused by rapid and high-frequency movements.

C. SpO₂ and Hemoglobin Calculations

To estimate SpO_2 levels, we used both AC and DC data from the red and IR color channels to calculate the intermediate variable R using (2).

$$R = \frac{I_{AC,red}/I_{DC,red}}{I_{AC,IR}/I_{DC,IR}} \quad (2)$$

To calibrate the device, we obtained a calibration curve relating R values to SpO_2 levels from the literature [32]. However, it should be noted that an appropriate calibration curve requires either human or animal experiments in a controlled environment, utilizing several strategies to induce extremely low-oxygenation levels on the patients without significant harm [27], [33].

To find the changes in the hemoglobin oxygenation levels (ΔHbR and ΔHbO_2), we used a modified version of the Beer-Lambert Law with scattering approach [34]. Equations (3) and (4) indicate this modified mathematical model.

$$\Delta[HbR] = \frac{\epsilon_{HbO_2}(\lambda_2)\Delta\mu_a(\lambda_1) - \epsilon_{HbO_2}(\lambda_1)\Delta\mu_a(\lambda_2)}{\epsilon_{HbR}(\lambda_1)\epsilon_{HbO_2}(\lambda_2) - \epsilon_{HbO_2}(\lambda_1)\epsilon_{HbR}(\lambda_2)} \quad (3)$$

$$\Delta[HbO_2] = \frac{\epsilon_{HbR}(\lambda_1)\Delta\mu_a(\lambda_2) - \epsilon_{HbR}(\lambda_2)\Delta\mu_a(\lambda_1)}{\epsilon_{HbR}(\lambda_1)\epsilon_{HbO_2}(\lambda_2) - \epsilon_{HbO_2}(\lambda_1)\epsilon_{HbR}(\lambda_2)} \quad (4)$$

$\Delta\mu_a(\lambda_x)$ represents the change in absorption at specific wavelength. ϵ_{HbO_2} and ϵ_{HbR} refer to the molar absorptivity of oxyhemoglobin and deoxyhemoglobin, respectively. Considering that oxyhemoglobin and deoxyhemoglobin are the only chromophores involved, the change in absorption at a particular wavelength can be calculated using the differential pathlength factor and the variation in light intensity (see (5)).

$$\Delta\mu_a(t) = \frac{-\ln\left(\frac{I_t}{I_{t-1}}\right)D}{DPF} \quad (5)$$

I_t and I_{t-1} represent the measured light intensity values at time and the preceding time step, respectively. D refers to the source detector distance, and the differential pathlength factor to DPF . Substituting (5) into (3) and (4), yielding to obtain the change in concentration of deoxyhemoglobin, and oxyhemoglobin represented by (6) and (7).

$$\Delta[HbR] = \frac{\epsilon_{HbO_2}(\lambda_2)\frac{-\ln\left(\frac{I_t(\lambda_1)}{I_{t-1}(\lambda_1)}\right)}{DPF(\lambda_1)} - \epsilon_{HbO_2}(\lambda_1)\frac{-\ln\left(\frac{I_t(\lambda_2)}{I_{t-1}(\lambda_2)}\right)}{DPF(\lambda_2)}}{\epsilon_{HbR}(\lambda_1)\epsilon_{HbO_2}(\lambda_2) - \epsilon_{HbO_2}(\lambda_1)\epsilon_{HbR}(\lambda_2)} \quad (6)$$

$$\Delta[HbO_2] = \frac{\epsilon_{HbR}(\lambda_1)\frac{-\ln\left(\frac{I_t(\lambda_2)}{I_{t-1}(\lambda_2)}\right)}{DPF(\lambda_2)} - \epsilon_{HbR}(\lambda_2)\frac{-\ln\left(\frac{I_t(\lambda_1)}{I_{t-1}(\lambda_1)}\right)}{DPF(\lambda_1)}}{\epsilon_{HbR}(\lambda_1)\epsilon_{HbO_2}(\lambda_2) - \epsilon_{HbO_2}(\lambda_1)\epsilon_{HbR}(\lambda_2)} \quad (7)$$

D. Benchtop Experiments

To test the functionality of the wearable device, we designed a straightforward benchtop experiment based on our previous work to evaluate the performance of the ZVS circuit and how the NIRS sensor activates the entire system [29]. Fig. 3 illustrates the

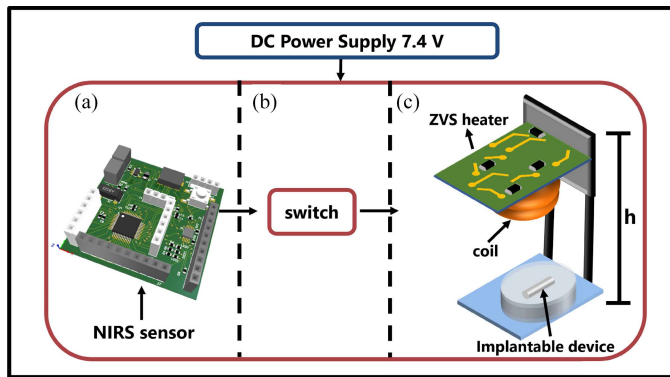


Fig. 3. Block diagram of the components implemented for the benchtop experiments. (a) Schematic of the front side of the NIRS device. We activated a digital pin of the microcontroller to drive the switch and the ZVS module; (b) representation of the MOSFET switch driver to integrate the instrumentation circuit to the ZVS driver; (c) diagram of electromagnetic field generator, placed at different height levels to melt the PCM of our minimally invasive capsule.

main components involved in the experiment. We programmed the microcontroller to manually activate the Dual MOSFET switch and the ZVS circuit. We used a commercial DC power supply (Agilent E366454 A DC Power Supply, Agilent Scientific Instrument, Inc, Santa Clara, CA, USA) to power the electronic components. We followed the same protocols stated in our previous work to test the electromagnetic field generator and its effect on melting the phase change material (PCM) used in the fabrication process of our minimally invasive implantable drug delivery capsule [29].

E. Human Test Trials

To evaluate the capabilities of the NIRS sensor to detect BAO-driven hypoxia events, we designed a test based on BAO using a conventional sphygmomanometer with a total of eight volunteers. The human subject research was approved by Purdue University's Institutional Review Board (Protocol #IRB-2020-297). To gather the subjects, we established the criteria of participation on the test as follows: (i) the participant must be at least 18 years old or older; (ii) the participant must have a no history of any cardiovascular disease or events that compromise the regular functionalities of the respiratory system; (iii) the patient cannot be an opioid user; and (iv) the patient must be conscious and free or any hallucinogens, substances or medication that compromise the cognitive system during the test.

The subjects were tested for six BAO events. During the trial, we asked the volunteers to sit comfortably, keeping the right arm and the feet well supported. Both feet rested flat on the floor and the right hand was placed over a table as indicated in Fig. 4(a). We tightened the wearable device on the subject and placed the bracelet cuff over the upper part of the arm, surrounding the brachial artery.

The test consisted of three main events (Fig. 4(b)) with a total duration of 180 s. Event (1): We asked the subjects to rest for 60 s, breathing without forced episodes, avoiding abrupt movements of the wrist. Event (2): We induced a low oxygen event by a BAO test. The occlusion was caused due to a continuous pressure of

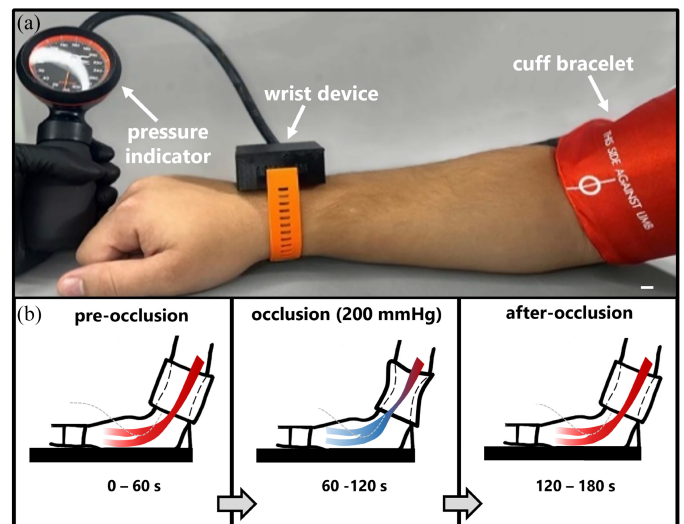


Fig. 4. Set up for the BAO trial mimicked with a conventional sphygmomanometer. Events during human trials: event (1): pre-occlusion section for a range of 60 seconds of resting time; event (2): low oxygen event due to BAO at 200 mmHg of pressure induced through the bracelet cuff; event (3): resting period after the BAO. The scale bar of this figure indicates 2 cm.

200 mmHg on the bracelet cuff for 60 s. After the test was completed, the pressure over the arm was released, following the comfort state of the patient throughout the trial. Event (3): We asked the subjects to rest for 60 s after the pressure over the arm was fully released.

F. Statistical analysis

To compare the statistical significance of the data among the groups of interest for the pre-occlusion, BAO, and post-occlusion, we conducted a one-way ANOVA Games-Howell test with a significance level ($\alpha = 0.05$). We defined three groups of interest for each set of data containing these variables as follows: (1) red light intensity peak-peak databits, (2) IR light intensity peak-peak databits, (3) ΔHbO_2 calculated values, (4) ΔHbR calculated values, and (5) SpO_2 obtained levels for each group. To analyze the data, we used an open-source statistics program (*R*, V.4.2.2).

G. Noise Level Characterization: Signal-to-Noise Ratio (SNR) - Power Supply Noise and Other Artifacts

In order to evaluate the noise level of the output signals, we calculated the SNR of the data related to the physiological aspects and oxygenation of the patients during the human experiments. We analyzed each set of data for the SNR of the ΔHbR , ΔHbO_2 , and SpO_2 signals from the brachial occlusion human trails. To determine the noise levels, we analyzed these signals by using MATLAB (R2023a, Mathworks, Inc. Natick, MA, USA).

To quantify the noise from the power supply of the wearable within an operating frequency range, we conducted experiments in two steps. The first step involved eliminating the source of external noise by using a fully shielded chamber (Controlled

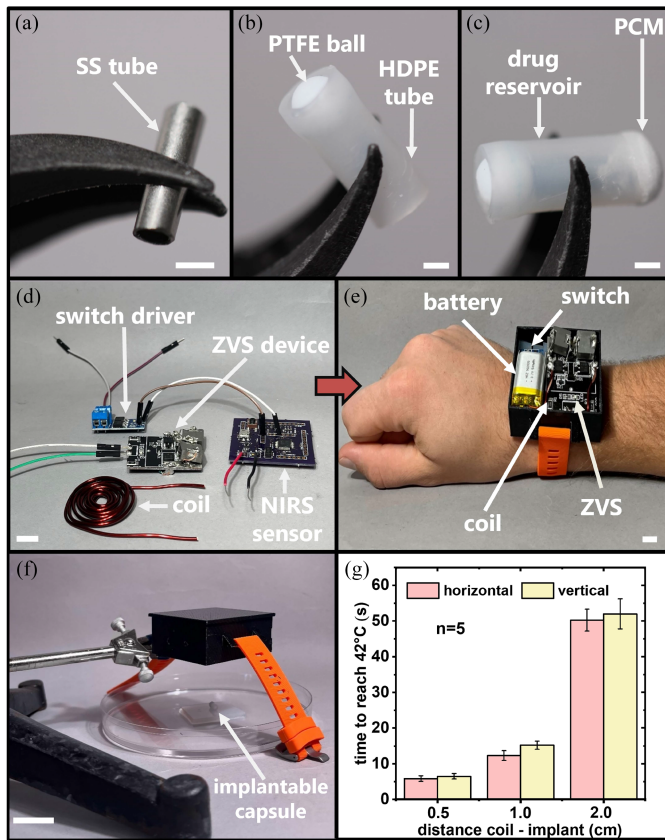


Fig. 5. Design, fabrication, and testing of the NIRS wearable device. (a) SS heating element tube (b) HDPE tube and a PTFE sealing ball. (c) Final prototype of the drug reservoir sealed with PCM. (d) List of electronic components of the wearable device. (e) A fully assembled wearable device on a subject. (f) Evaluation of the wearable device to test the ZVS driver at different heights above the drug delivery capsule. (g) Time for the implantable drug delivery device to reach 42 °C at different distances. The scale bars for (a-c) is 1 mm; (d) is 1 cm; (e) is 5 mm; and (f) is 2 cm.

Acoustical Environments, Industrial Acoustics Company, Inc). During the initial stage of the trials, we measured the noise levels from three PCB NIRS and ZVS heaters five times each ($n = 15$) within the two frequency ranges (30 kHz–300 kHz @swp 133 ms & 300 kHz–3 GHz @swp 3 ms) using a commercial handheld RF spectrum analyzer (N9913 A FieldFox Handheld RF Analyzer, 4 GHz, Keysight Technologies, Inc, Santa Rosa, CA, USA). Subsequently, we measured the V_{rms} noise of the power supply using an oscilloscope (Mixed Signal Oscilloscope MSOX2024 A, 200 MHz, Keysight Technologies, Inc, Santa Rosa, CA, USA). We conducted the measurement for 30 s, five times for each PCB NIRS and ZVS heater ($n = 15$).

III. RESULTS

A. Design and Fabrication

Figs. 5(a)–(c) show the implantable device made using fully biocompatible materials as previously reported [29]. Fig. 5(d) shows the subcomponents for the final wearable device that includes the NIRS sensor, a microcontroller, a TIA circuit, a voltage regulator, and a 16-bit ADC.

To couple the sensing elements with the high-power electromagnetic actuator, we modified the commercial MOSFET driver switch. Fig. 5(d) shows the device with an absence of the header-wire-to-board, with the aim of reducing the size of switch to facilitate the packaging of the entire components in a 3D printed wrist case with measurements of 59 mm × 49 mm × 25 mm. The modified ZVS driver features a volume of 32 mm × 41 mm × 3 mm, which is 90% approximately smaller in height than the commercial electromagnetic field generator we used in our previous work (see Figs. 5(d), and (e)). This modified version reached 14.8 kA/m of magnetic field at 195 kHz, delivering the necessary power capabilities.

B. Benchtop Experiments

We evaluated the drug release capability of our wearable device through a benchtop experiment. We activated the drug reservoir at various orientations and heights, following the methodology from our previous work [29] (see Fig. 5(f)). Fig. 5(g) shows the time for the heating element to reach 42 °C at different orientations and heights. As expected, shorter distances between the coil and the heating element led to a faster time to the melting temperature. At a distance of 0.5 cm, the activation times were 5.84 ± 0.82 s horizontally and 6.48 ± 0.76 s vertically ($n = 5$ for each orientation). However, as the gap between the coil and the heater increased, the time needed to achieve the target temperature increased significantly, highlighting a potential limitation of our system.

C. Human Experiments and Statistical Analysis

Fig. 6 shows the set of results from the human experiments conducted before, during, and after the occlusion events. Fig. 6(a)–(c), and d highlight the peak-peak values and transient graphics for the light emitters during and after the BAO events, respectively. Fig. 6(a), and (b) demonstrate significant statistical differences among the groups before and after occlusion in relation to the BAO event for IR peak-peak values ($p < 0.001$ and $p < 0.001$). During non-occlusion events, there is dominant absorption of IR light due to higher oxygen availability in the capillaries, with average values of 61.06 ± 3.56 before occlusion and 60.02 ± 5.81 after occlusion. Conversely, during occlusion, there is a sharp decrease in IR light absorption to 30.25 ± 6.42 as deoxygenation becomes more prominent in the blood, which is evident from its transient curve (see Fig. 6(a)). Similarly, Figs. 6(c), and (d) demonstrate statistical significance for red intensity peak-peak values among the groups before and after occlusion in relation to the BAO event ($p < 0.001$ and $p < 0.001$). Since the red light has a strong affinity and characteristics with HbR , we observe low light intensity during the non-occlusion events of 27.90 ± 2.81 (before the BAO) and 27.71 ± 4.99 (after the BAO). This is followed by a sharp increase in intensity during the BAO episode (55.31 ± 6.94). Fig. 6(c) illustrates the transitional behavior for red light during the human trials, showing a noticeable increase in magnitude during the BAO event as the oxygen in the capillaries becomes less prominent.

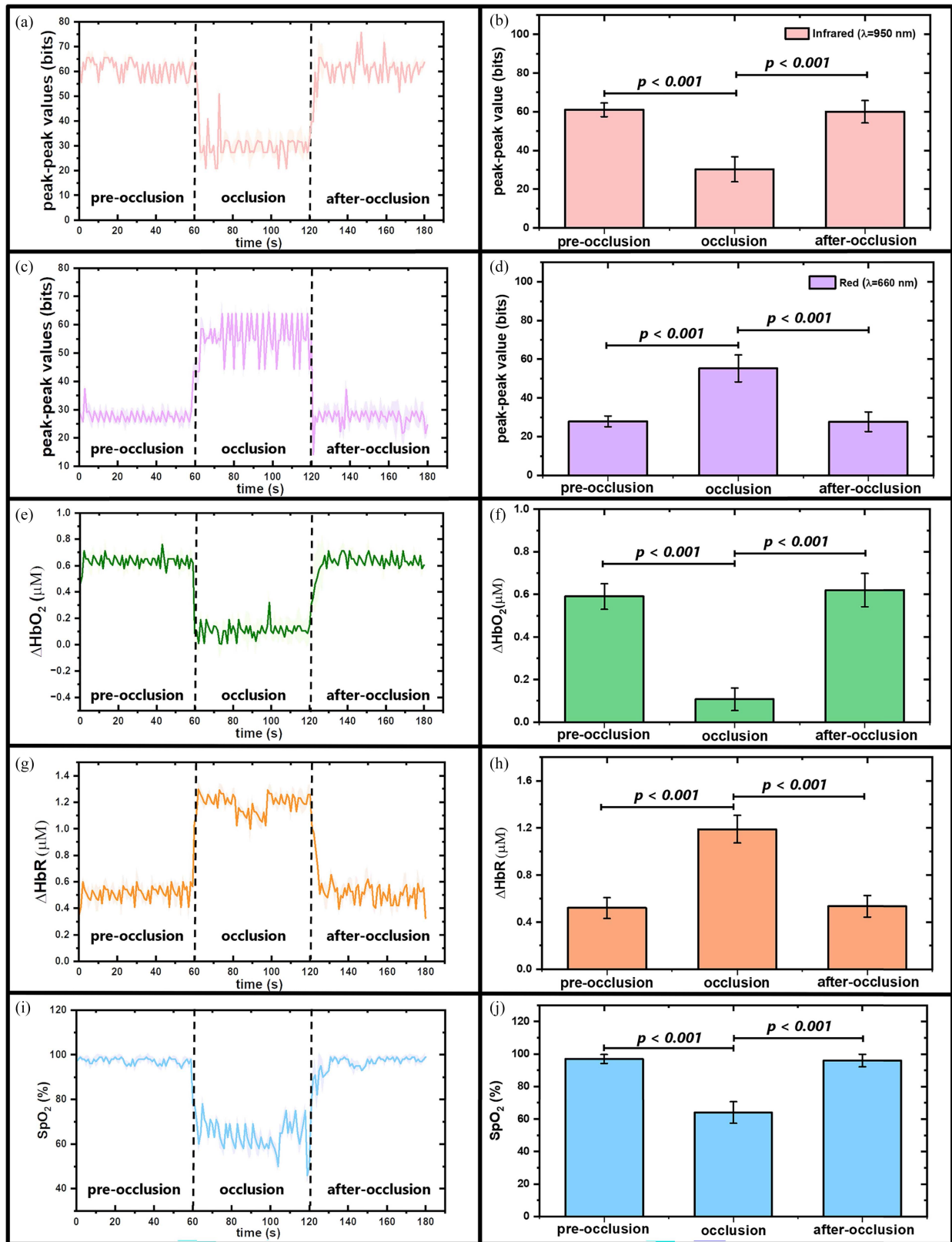


Fig. 6. Human Experiments results and statistical analysis before, during and after the BAO trials. (a) Representative transient Infrared light intensity peak-peak values during a BAO experiment. (b) Infrared light intensity peak-peak values during the human trials: before, during and after the BAO events. (c) Representative transient red light intensity peak-peak values during a BAO experiment. (d) Red light intensity peak-peak values during the human trials: before, during and after the BAO events. (e) Representative transient ΔHbO_2 concentration values during a BAO experiment. (f) ΔHbO_2 concentration values for pre-occlusion, during occlusion and after-occlusion. (g) Representative transient ΔHbR concentration values during a BAO experiment. (h) ΔHbR concentration values for pre-occlusion, during occlusion and after-occlusion. (i) Representative transient SpO_2 values during a BAO experiment. (j) SpO_2 levels during the human trials.

To analyze the oxygenation processes during the BAO trials, a clear understanding of the changes in hemoglobin oxygenation is crucial. Figs. 6(e), and (f) depict changes in HbO_2 , while Fig. 6(g), and 6(h) show the variation in HbR , respectively, with statistical significance observed among the groups before and after occlusion with respect to the BAO episodes during the human trials ($p < 0.001$ and $p < 0.001$). As expected, ΔHbR and ΔHbO_2 exhibit opposite variations, particularly during the BAO event due to the gas exchange process in the capillaries. Figs. 6(e),(f) show a negative decrease in the oxygenation concentration for HbO_2 , as the occlusion takes place, reaching average values of $0.12 \pm 3.56 \mu\text{M}$, whereas non-occlusion events display insignificant changes in concentration ($0.59 \pm 0.06 \mu\text{M}$ and $0.62 \pm 0.07 \mu\text{M}$), respectively. Conversely, Figs. 6(g), and (h) reveal a positive increase in HbR concentration during the BAO event ($1.19 \pm 0.12 \mu\text{M}$), followed by a steady decrease in concentration during the non-occlusion cases ($0.52 \pm 0.08 \mu\text{M}$ and $0.53 \pm 0.09 \mu\text{M}$).

Ultimately, Fig. 6(i), and 6(j) illustrate the SpO_2 values obtained during the BAO trials. Prior to occlusion, the oxygenation levels were $96.95 \pm 2.75\%$, followed by a sharp decrease to $64.08 \pm 6.61\%$ during the BAO episode due to low oxygenation in the brachial artery, resulting in inadequate perfusion of HbO_2 in the capillaries. The re-oxygenation event after the BAO episode is noticeable with SpO_2 values of $95.98 \pm 3.86\%$. The statistical differences among the oxygenated events with the BAO episode were $p < 0.001$ and $p < 0.001$, respectively. Fig. 6(i) depicts the transitional graph for the SpO_2 levels during the human trials. During the pre-occlusion stage, the oxygenation levels do not exhibit abrupt fluctuations, as expected in normal blood oxygen flow within the subjects under normal respiratory conditions. A noticeable sharp decrease in the SpO_2 levels occurs after a few seconds of the occlusion trial (around 62 s), indicating a successful induction of low oxygenation. During this occlusion stage, the oxygenation in the subjects does not exceed values above 90%, which corresponds to the defined threshold for a hypoxia-driven opioid overdose. Finally, the after-occlusion event highlights a prominent increase in the oxygenation levels around 121 s, indicating a normal recovery process in blood perfusion within the volunteers until the end of the trial.

D. Noise Characterization

Fig. 7 shows the noise induced by the wearable device during the frequency sweep. We observed fluctuations in two distinct frequency spectra. There is a noise fluctuation within the power density amplitude range of 160 kHz to 220 kHz, exhibiting variations from approximately -3.26 dB to 3.49 dB. Moreover, we saw high-frequency jitters between 11 MHz and 3 GHz, with variations from -3.51 dB to 4.17 dB. Finally, V_{rms} noise values for the power supply was measured at $268.83 \text{ mV} \pm 13.91 \text{ mV}$. It is important to note that these fluctuations might be deemed negligible given that the devices uses 7.4 V as the power supply.

We also calculated the SNR of the ΔHbR , ΔHbO_2 , and SpO_2 signals gathered during the brachial occlusion experiments with human subjects. The changes in hemoglobin oxygenation signals, ΔHbR and ΔHbO_2 , resulted in SNR of

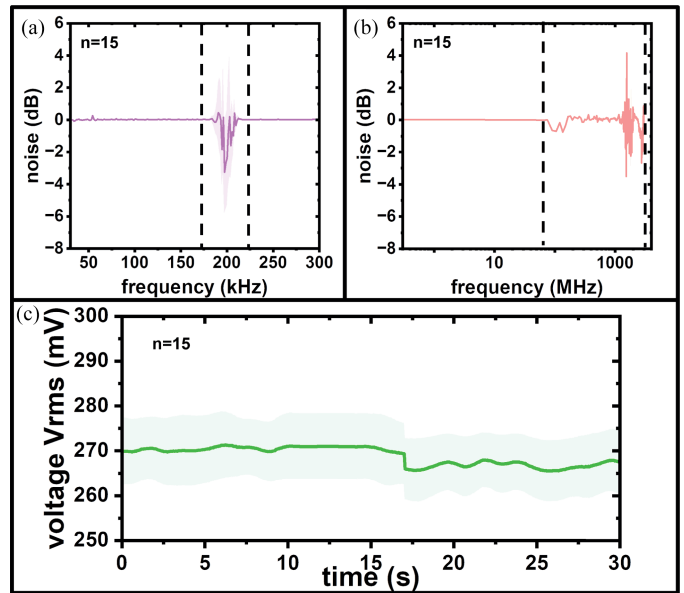


Fig. 7. Noise induced by the wearable device within two frequency spectra and V_{rms} noise from the power supply. (a) Noise level between 30 kHz - 300 kHz. (b) Noise level between 300 kHz - 3 GHz. (c) V_{rms} noise of the power supply.

2.27 dB and 8.71 dB, respectively. The SNR for SpO_2 was 7.24 dB.

IV. DISCUSSION

Opioid overdose is a prominent public health issue with devastating consequences that can be prevented and mitigated through the invention of novel technologies and engineered solutions. In this study, we introduced a proof-of-concept closed-loop wearable device for the detection of BAO-driven hypoxia events and the delivery of the life-saving antidote, naloxone. Our vision is to develop a wearable wrist device that improves usability by significantly reducing the size of the electronics.

Although there are other reports of closed-loop drug delivery systems for opioid overdose, we believe this is the first demonstration of utilizing NIRS to detect and treat an overdose event (see Table I for a detailed comparison with the state of the art in wearable devices for opioid-overdose detection and treatment). Imitiaz et al. proposed a closed-loop wearable device based on a conventional oximeter to detect potential opioid-overdose episodes [21]. This wearable system was not fully tested, particularly in terms of its sensing capabilities. Our preliminary data reveal the potential of our device to detect hypoxia cardiorespiratory events using NIRS. Figs. 6(i), and (j) depict SpO_2 average values $< 90\%$ during the occlusion episode, which can be attributed to a low-oxygenation event induced by the BAO. These results are also supported by the low peak-peak values of IR intensity (see Fig. 6(a), and (b)) and the higher peak-peak intensity values of the red light (see Fig. 6(c), and (d)) during the low oxygenation events. As aforementioned, red light exhibits more absorption affinity with HbR , indicating reduced oxygen availability in the capillaries. The inverse absorbance properties of the IR light, in contrast to red light, provide a better understanding for identifying the dominant presence of

TABLE I
COMPARISON OF THE STATE OF THE ART IN WEARABLE TECHNOLOGIES FOR OPIOID-OVERDOSE DETECTION AND TREATMENT

Ref (Year)	Opioid Detection Method	Closed-loop (Y/N)	Research vs Commercial	Actuation Method (Delivery of Naloxone)	Validation Method (Human/Animal Studies, Benchtop and/or In Silico)
This work (2023)	A wrist-worn wearable device capable of detecting hypoxia-driven opioid-overdose related events through NIRS	Yes	Research	A fully implantable capsule activated by a ZVS electromagnetic heater	Benchtop experiments and a NIRS sensor validated through human studies
[35] (2022-2023)	An FDA-approved disposable fingerprint-based sensor to detect hypoxia events and pulse rate, including a mobile App for data recording and tracking	No	Commercial Opioid Halo™, Masimo (NASDAQ: MASI)	N/A	N/A
[21] (2021)	SpO_2 (hypoxia events)	Yes	Research	A modified needle-based injector system	In silico experiments
[16] (2021)	Apnea detection and respiratory rate through an accelerometer-based sensor patch	Yes	Research	A commercial needle-based wearable injector	Human studies under controlled clinical settings
[36] (2021)	Respiratory rate through an attachable pressure sensor onto a face-mask	No	Research	N/A	Benchtop experiments
[37] (2020)	A wearable microneedle array for electrochemical continuous opioid sensing	No	Research	N/A	Benchtop experiments (skin-mimicking phantom gel)
[29] (2019)	Respiratory rate through a commercial wearable ECG sensor	Yes	Research	An implantable capsule and an electromagnetic heater	Animal studies and benchtop experiments
[19] (2016)	PPG, EDA, skin temperature and respiratory rate along with a tri-axis accelerometer	No	Commercial (Empatica E4, Empatica, Inc, Cambridge, MA, USA)	N/A	Human studies tested by [38], [39]
[15] (2015)	EDA, skin temperature and respiratory rate along with a tri-axis accelerometer	No	Commercial (Q sensor™, Affectiva, Inc, Boston, MA, USA). This device is no longer available in the market*	N/A	Human studies tested by [15], [18]

oxygen in the capillaries. It is crucial to highlight that during the occlusion event, the average SpO_2 levels drastically dropped to $64.08 \pm 6.61\%$ (see Fig 6(i), and (j)). These results cannot be fully corroborated in a real scenario of a low-oxygenation stage. In a person, oxygenating at levels $< 90\%$, symptoms such as dizziness, bluish skin, and unconsciousness can be easily perceived [21], [28], indicating the need of immediate medical assistance. We acknowledge the limitation of our device to accurately measuring low oxygen levels, as we relied on calibration curves for the R and SpO_2 from the literature, which may not precisely align with the outcomes of our NIRS sensor.

Regarding the transitional results for the oxygenation levels, we obtained preliminary data to serve as a baseline for detecting an opioid overdose event (see Fig. 6(i), and (j)). During the pre-occlusion stage, we observed small fluctuations in the SpO_2 levels above 96%, indicating regular oxygenation in the capillaries. After inducing the BAO event, we observed a drop in SpO_2 levels at approximately 62 s, successfully inducing

a period of low oxygenation. It is important to highlight that our device is capable of detecting the hypoxia-driven event in less than 2 seconds. However, further studies are required to verify the detection of the overdose due to the limitations of the BAO, which simulates a localized hypoxia environment. As expected, during the BAO event, the SpO_2 values were below 90%, indicating poor oxygenation in the capillaries. We observed abrupt variations during the BAO stage, which could be attributed to different factors. We believe that the conditions of each patient during the low-oxygenation process are slightly different, depending on their cardiorespiratory capacity to recover and address poor oxygenation perfusion in the brachial artery. Another aspect to consider is that our device calibration method does not consider values lower than 60%, as our main focus is on a threshold below 90% to activate the delivery of the life-saving antidote. Lastly, our data allowed us to observe the recovery process of re-oxygenation in the capillaries after releasing the cuff pressure. At approximately 121 s, we detected an abrupt

increase in the oxygenation levels, as expected in subjects with no significant cardiorespiratory alterations. We believe that the variations during the re-oxygenation process are due to the different conditions of each patient's cardiorespiratory capacity, which can be influenced by factors such as diet, exercise, and other routines [28], [40].

Another critical aspect to analyze is the influence of human and other confounding factors that could limit the sensing capabilities of our system. Skin tone is a widely known confounding factor during optical sensing applications, and its effect on the accuracy of oximetry approaches has been extensively studied [41], [42]. However, there is still a considerable gap regarding the bias induced by melanin and skin color in oximetry measurements, which requires additional analysis of specific factors in terms of absorbance and light penetration constraints. Another crucial factor to consider is skin pressure, which may be related to the tightness level of the wrist-wearable device. The photodetector of our device should be firmly pressed onto the skin without generating blanching on the skin tissue. Excessive pressure can modify the oxygenation levels in the sensing area of the skin due to the disruption of blood flow, leading to defective measurements by our device [43]. Lastly, other factors such as EDA, skin temperature, and movement artifacts could strongly affect the measurement capabilities of our device and should be further analyzed and identified through additional experiments and enhancements in the instrumentation of our device.

Taking into account the drug delivery system of our wearable device, we did not find other studies that utilizes a similar approach. Most of the current research studies for closed-loop wearable devices focused on commercial wearable injectors [16], [21]. In these scenarios the injectors may be bulky and have some limitations that could lead to infections, needle phobia and other factors, leading to unwillingness of the opioid users to wear a wearable device due to stigma associated with opioid use disorder. Our hope is that the wrist-worn device popularized by many consumer electronics, will alleviate potential concerns of wearability and increase the compliance of opioid use disorder (OUD) patients. However, future studies are needed to evaluate the willingness of opioid users to wear wrist-based devices as a potential harm reduction strategy.

We noted noise fluctuations within the operational range of 195 kHz (Fig. 7(a)). Such fluctuations is anticipated, given by the electromagnetic heater. For our application, it is crucial to eliminate high-frequency artifacts since the PPG signals predominantly exist in a low-frequency spectrum, as referenced in [44]. This may be addressed by integrating advanced digital filtering techniques. Furthermore, the high-frequency noise artifacts (Fig. 7(b)) may be from the LEDs of the wearable's light source since their operational frequency corresponds to this range. To fully characterize the sources of the noise from real-world usage, we need additional human trials to assess the impact of various confounding factors like skin color, strap tightness, and sweat levels on the sensing area, among others. In terms of the V_{rms} noise (Fig. 7(c)), the voltage fluctuations are negligible relative to the power supply values. However, a deeper analysis of these voltage fluctuations and their impact on the device's output signals may be warranted to ensure safe and

reliable operations in humans. Finally, as we believe our work is the first demonstration of utilizing NIRS to detect an BAO event, the obtained SNR values require a further comparison with clinical grade equipment. In the future, optimization in signal processing techniques may be needed as well to balance between computational requirements, power supply, and the addition of analog components to our device. For this aspect, we will need to obtain signals with a higher SNR, similar to other works [45], [46].

In terms of the drug delivery, our device is capable of ensuring a rapid delivery of a burst of the life-saver antidote. For both vertical and horizontal alignments (5.84 ± 0.82 s vs 6.84 ± 0.76 s at 0.5 mm distance), the system could reach the appropriate temperature (42°C) to melt the PCM on time, allowing the delivery of the drug as quickly as possible. Also, it is important to note that the fast response for the horizontal orientation of the implantable capsule could be due to the nonaxial component of the electromagnetic field, causing eddy currents over the implantable capsule. However, it is important to highlight the limitations of our system that are attributed to higher distances between the capsule and the electromagnetic heater as evidenced in Fig 5(g). Additionally, further studies are required to evaluate the influence of the induced temperatures by the ZVS on the tissue during the activation of the PCM to deliver naloxone.

The main goal of this work is to provide a reliable closed-loop fully wearable device to detect an opioid overdose-induced hypoxia cardiorespiratory event, capable of delivering a burst dose of naloxone as quickly as possible. Our results showed that the electromagnetic actuator is capable of releasing the drug within 10 s at closer distances under the skin. In terms of the NIRS sensing component, future research is needed not only in terms of the detection of changes in HbO_2 and HbR , but also to address the aforementioned issues due to human factors and calibration of the device [41]. Also, further enhancements in terms of electronics are needed to optimize the post digital processing, reduce the power consumption of the device, and strategize alternatives for noise reduction.

V. CONCLUSION

Herein, we demonstrated the design, fabrication, and evaluation of a wrist-wearable device for sensing changes in blood oxygenation levels and actuating a drug deliver capsule based on three well-defined components: (i) a NIRS sensor, (ii) a MOSFET dual switch, and (iii) a modified ZVS circuit. Our experiments demonstrated the capability of the NIRS to measure changes in hemoglobin concentration (HbO_2 and HbR) and detect a simulated opioid overdose event through a BAO-hypoxia driven test in less than 2 s. Furthermore, our preliminary data revealed the ability of our system to rapidly release the antidote from our previous minimally invasive capsule, enabling a rapid response during an opioid overdose. Future experiments are planned to improve the performance of the device by addressing a few shortcomings. First, we will integrate analog-digital filters and signal data processing resources to mitigate limitations caused by human factors such as induced movement artifacts and variations in skin tone, which may worsen the performance of our device. Second, we will further miniaturize and optimize the electronics, reducing the size of the device as much as possible to

improve usability and power consumption. Our ultimate vision is that such a device could be used to help mitigate the devastatingly high rates of opioid overdose and in other potential emergency drug delivery applications.

REFERENCES

- [1] Centers for Disease Control and Prevention, "The Drug overdose epidemic: Behind the numbers," 2023. Accessed: Oct. 31, 2023, [Online]. Available: <https://www.cdc.gov/opioids/data/>
- [2] National Institutes of Health, "Drug overdose death rates," 2023. Accessed: Oct. 31, 2023, [Online]. Available: <https://nida.nih.gov/research-topics/trends-statistics/overdose-death-rates>
- [3] J.-X. Li, "Combining opioids and non-opioids for pain management: Current status," *Neuropharmacology*, vol. 158, 2019, Art. no. 107619, [Online]. Available: <https://doi.org/10.1016/j.neuropharm.2019.04.025>
- [4] Centers for Disease Control and Prevention, "Opioid basics," 2023. Accessed: Aug. 16, 2023, [Online]. Available: <https://cdc.gov/opioids/basics/index.html>
- [5] B. Cohen, L. J. Ruth, and C. V. Preuss, "Opioid analgesics," 2023. Accessed: Aug. 16, 2023, [Online]. Available: <https://www.ncbi.nlm.nih.gov/books/NBK459161/>
- [6] T. Yamanaka and R. T. Sadikot, "Opioid effect on lungs," *Respirology*, vol. 18, no. 2, pp. 255–262, 2013, doi: [10.1111/j.1440-1843.2012.02307.x](https://doi.org/10.1111/j.1440-1843.2012.02307.x)
- [7] M. J. Emery, C. C. Groves, T. N. Kruse, C. Shi, and G. Terman, "Ventilation and the response to hypercapnia after morphine in opioid-naïve and opioid-tolerant rats," *Anesthesiology*, vol. 124, no. 4, pp. 945–957, 2016, doi: [10.1097/ALN.0000000000000997](https://doi.org/10.1097/ALN.0000000000000997)
- [8] J. Manikkath and J. A. Subramony, "Toward closed-loop drug delivery: Integrating wearable technologies with transdermal drug delivery systems," *Adv. Drug Del. Rev.*, vol. 179, 2021, Art. no. 113997.
- [9] L. V. Shaw et al., "Naloxone interventions in opioid overdoses: A systematic review protocol," *Systematic Rev.*, vol. 8, pp. 1–9, 2019.
- [10] U.S. Food and Drug Administration, "FDA approves first over-the-counter naloxone nasal spray," 2023. Accessed: Nov. 13, 2023, [Online]. Available: <https://www.fda.gov/news-events/press-announcements/fda-approves-first-over-counter-naloxone-nasal-spray>
- [11] B. L. Hanson, R. R. Porter, A. L. Zöld, and H. Terhorst-miller, "Preventing opioid overdose with peer-administered naloxone: Findings from a rural state," *Harm Reduction J.*, vol. 17, pp. 1–9, 2020.
- [12] D. P. Wermeling, "Review of naloxone safety for opioid overdose: Practical considerations for new technology and expanded public access," *Therapeutic Adv. Drug Saf.*, vol. 6, no. 1, pp. 20–31, 2015.
- [13] E. W. Boyer, "Management of opioid analgesic overdose," *New England J. Med.*, vol. 357, no. 2, pp. 146–155, 2012.
- [14] National Institute on Drug Abuse, "Naloxone for opioid overdose: Life-Saving science," 2017. Accessed Aug. 16, 2023, [Online]. Available: <https://archives.nida.nih.gov/publications/naloxone-opioid-overdose-life-saving-science>
- [15] S. Carreiro et al., "Real-time mobile detection of drug use with wearable biosensors: A Pilot Study," *J. Med. Toxicol.*, vol. 11, no. 1, pp. 73–79, 2015.
- [16] J. Chan et al., "Closed-loop wearable naloxone injector system," *Sci. Rep.*, vol. 11, no. 1, 2021, Art. no. 22663.
- [17] T. Y. Abay and P. Kyriacou, "Photoplethysmography for blood volumes and oxygenation changes during intermittent vascular occlusions," *J. Clin. Monit. Comput.*, vol. 32, no. 3, pp. 447–455, 2018.
- [18] M. S. Mahmud, H. Fang, H. Wang, S. Carreiro, and E. Boyer, "Automatic detection of opioid intake using wearable biosensor," in *Proc. Int. Conf. Comput., Netw., Commun.*, 2018, pp. 784–788.
- [19] Inc Empatica, "Meet EmbracePlus the E4 wristband's next-gen successor," 2023. Accessed: Nov. 13, 2023, [Online]. Available: <https://www.empatica.com/en-int/research/e4/>
- [20] R. Singh, B. Lewis, B. Chapman, S. Carreiro, and K. Venkatasubramanian, "A machine learning-based approach for collaborative non-adherence detection during opioid abuse surveillance using a wearable biosensor," in *Proc. Biomed. Eng. Syst. Technol., Int. Joint Conf., BIOSTEC Revised Sel. Papers*, 2019, vol. 5, pp. 310–318.
- [21] M. S. Intiaz, C. V. Bandoian, and T. J. Santoro, "Hypoxia driven opioid targeted automated device for overdose rescue," *Sci. Rep.*, vol. 11, no. 1, 2021, Art. no. 24513.
- [22] T. Y. Abay and P. A. Kyriacou, "Investigation of photoplethysmography and near infrared spectroscopy for the assessment of tissue blood perfusion," in *Proc. Annu. Int. Conf. IEEE Eng. Med. Biol. Soc. IEEE Eng. Med. Biol. Soc. Annu. Int. Conf.*, 2014, pp. 5361–5364.
- [23] N. F. Agbangla, P. Maillot, D. Vitiello, and P. Herman, "Mini-review of studies testing the cardiorespiratory hypothesis with near-infrared spectroscopy (NIRS): Overview and perspectives," *Front. Neurosci.*, vol. 15, pp. 1–7, 2021.
- [24] C. W. Hogue, A. Levine, A. Hudson, and C. Lewis, "Clinical applications of near-infrared spectroscopy monitoring in cardiovascular surgery," *Anesthesiology*, vol. 134, no. 5, pp. 784–791, 2021.
- [25] P. Kainan, A. Sinchai, P. Tuwanut, and P. Wardkein, "New pulse oximetry detection based on the light absorbance ratio as determined from amplitude modulation indexes in the time and frequency domains," *Biomed. Signal Process. Control*, vol. 75, 2022, Art. no. 103627.
- [26] T. W. Scheeren, P. Schober, and L. A. Schwarte, "Monitoring tissue oxygenation by near infrared spectroscopy (NIRS): Background and current applications," *J. Clin. Monit. Comput.*, vol. 26, no. 4, pp. 279–287, 2012.
- [27] Analog Devices, Inc, "Guidelines for SpO2 measurement," 2023. Accessed: Aug. 16, 2023, [Online]. Available: <https://www.analog.com/en/technical-articles/guidelines-for-spo2-measurement--maxim-integrated.html>
- [28] B. K. Peterson, "Chapter 22 – vital signs," M.H Cameron and L.G.B.T.-P.R. Monroe, Eds., Saint Louis: W.B. Saunders, 2007, pp. 598–624, doi: [10.1016/B978-072160361-2.50025-9](https://doi.org/10.1016/B978-072160361-2.50025-9).
- [29] B. Dhowan et al., "Simple minimally-invasive automatic antidote delivery device (a2d2) towards closed-loop reversal of opioid overdose," *J. Controlled Release*, vol. 306, pp. 130–137, 2019.
- [30] BioMon Sensor SFH7050, "OS-RAM Opto Semiconductors," version alpha.3, 2014. Accessed: Nov. 13, 2023, [Online]. Available: https://cdn.sparkfun.com/assets/8/3/f/6/e/SFH7050_datasheet.pdf
- [31] Texas Instruments, Inc, "OPA376 Precision (0.025mV), low noise (7.5nV/rtHz), low quiescent current (760uA) op amp," 2015. Accessed: Nov. 13, 2023, [Online]. Available: <https://www.ti.com/product/OPA376>
- [32] A. İ Bülbül and S. Küçük, "Pulse oximeter manufacturing and wireless telemetry for ventilation oxygen support," *Int. J. Appl. Math., Electron. Comput.*, vol. 4, no. 1, pp. 211–215, 2016.
- [33] N. A. Jumadi, G. K. Beng, M. A. M. Ali, E. Zahedi, and M. Morsin, "Development of theoretical oxygen saturation calibration curve based on optical density ratio and optical simulation approach," in *Proc. AIP Conf. Proc.*, 2017, vol. 1883, Art. no. 020024.
- [34] G. Strangman, M. A. Franceschini, and D. A. Boas, "Factors affecting the accuracy of near-infrared spectroscopy concentration calculations for focal changes in oxygenation parameters," *NeuroImage*, vol. 18, no. 4, pp. 865–879, 2003.
- [35] Masimo (NASDAQ: MASI), "Opioid halo™," 2023. Accessed: Oct. 31, 2023, [Online]. Available: https://opioidhalo.masimo.com/products/opioid-halo?utm_medium=cpc&utm_source=google&utm_campaign=moh-branded&gclid=Cj0KCQjwldKmBhCCARiAP-0rfz5UAsuH44I_8gRmhMqarMb10R9dYDNRDhLszlckNYJYvqP7nqkaAg0FEALw_wcB
- [36] L. Yang et al., "Wearable pressure sensors based on MXene/Tissue papers for wireless human health monitoring," *ACS Appl. Mater. Interfaces*, vol. 13, no. 50, pp. 60531–60543, 2021.
- [37] R. K. Mishra et al., "Continuous opioid monitoring along with nerve agents on a wearable microneedle sensor array," *J. Amer. Chem. Soc.*, vol. 142, no. 13, pp. 5991–5995, 2020.
- [38] F. I. S. García et al., "Using wearable technology to detect prescription opioid self-administration," *PAIN*, vol. 163, no. 2, 2022, pp. e357–e367.
- [39] B. P. Chapman, B. T. Gullapalli, T. Rahman, D. Smelson, E. W. Boyer, and S. Carreiro, "Impact of individual and treatment characteristics on wearable sensor-based digital biomarkers of opioid use," *NPJ Digit. Med.*, vol. 5, no. 1, 2022, Art. no. 123.
- [40] D. Neunh userer et al., "Impact of exercise training and supplemental oxygen on submaximal exercise performance in patients with COPD," *Scand. J. Med. Sci. Sports*, vol. 31, no. 3, pp. 710–719, 2021.
- [41] P. J. Colvonen, P. N. DeYoung, N.-O. A. Bosompra, and R. L. Owens, "Limiting racial disparities and bias for wearable devices in health science research?" *Sleep*, vol. 43, no. 10, 2020, Art. no. zsaal159.
- [42] E. R. Gottlieb, J. Ziegler, K. Morley, B. Rush, and L. A. Celi, "Assessment of racial and ethnic differences in oxygen supplementation among patients in the intensive care unit," *JAMA Intern. Med.*, vol. 182, no. 8, pp. 849–858, 2022.
- [43] W. Wang, C. P. Winlove, and C. C. Michel, "Oxygen partial pressure in outer layers of skin of human finger nail folds," *J. Physiol.*, vol. 549, no. Pt 3, pp. 855–863, 2003.
- [44] A. S. Karavaev et al., "Low-frequency component of photoplethysmogram reflects the autonomic control of blood pressure," *Biophysical J.*, vol. 120, no. 13, pp. 2657–2664, 2021.

- [45] F. Elsannah, A. Bilgaiyan, M. Affiq, C. H. Shim, H. Ishidai, and R. Hattori, "Reflectance-based organic pulse meter sensor for wireless monitoring of photoplethysmogram signal," *Biosensors*, vol. 9, no. 3, pp. 1–13, 2019.
- [46] S. Zauseder, A. Vehkaoja, V. Fleischhauer, and C. Hoog Antink, "Signal-to-noise ratio is more important than sampling rate in beat-to-beat interval estimation from optical sensors," *Biomed. Signal Process. Control*, vol. 74, 2022, Art. no. 103538.



Juan C. Mesa received the bachelor's degree in bioengineering from the Universidad de Antioquia, Medellin, Colombia, in 2020 (best GPA in his class). He is currently working toward the Ph.D. degree with the Laboratory of Implantable Microsystems Research, Weldon School of Biomedical Engineering, Purdue University, West Lafayette, IN, USA. He is also a STEM teacher for the diversity and inclusion extension program from Biomedical Engineering, Purdue University. His research interests include the development of wearable electronic devices for drug delivery applications.



Michael D. MacLean received the B.S. and M.S. degrees in biomedical engineering from Purdue University, West Lafayette, IN, USA. In 2018, he joined the Laboratory of Implantable Microsystems Research as a Graduate Researcher working on opioid overdose detection and automatic antidote delivery devices. He is currently as a Software Developer, Arcadia.io working on value-based care products. His research interests include biophotonic circuits, signal processing, and embedded systems.



María MS received the B.S. and M.S. degrees in industrial engineering with a concentration in electrical engineering from the University of Seville, Seville, Spain, in 2017 and 2019 respectively. In 2021, she was a Research Assistant in electrical engineering with Purdue University, West Lafayette, IN, USA. From 2019 to 2020, she was a Substation Electrical Engineer with Ayesa, Seville, Spain, where she worked on various projects designing electrical substation control and protections for Red Eléctrica de España (Spanish Electricity Grid). Her research inter-

ests include electric power and energy systems, simulations and modeling, and intelligent systems.



Alan Nguyen received the B.S. degree in biomedical engineering from Purdue University, West Lafayette, IN, USA during 2018–2021. He was with Indiana University's Pervasive Technology Institute, UITS Research Technologies, Bloomington, IN, in 2019, as a Research Affiliate under the National Science Foundation focusing on cloud-computing and 3D-visualization of veterinary medical data sets. He joined the Laboratory of Implantable Microsystems Research with the Weldon School of Biomedical Engineering, Purdue University during 2019–2021,

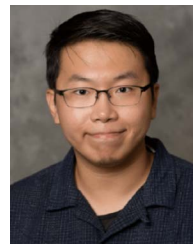
where he researched and tested detection mechanisms towards wearable-automated drug delivery devices.



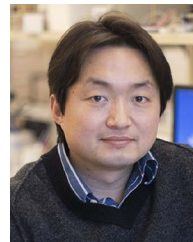
Rujuta Patel received the B.S. degree in biomedical engineering from Purdue University, West Lafayette, IN, USA, in 2021, and the M.S. degree in biomedical engineering from Duke University, Durham, NC, USA, in 2022. Her research interests include medical device design, sensors and wearable technologies for biomedical applications.



Timothy Diemer received the bachelor's degree in electrical engineering, (with a minor in business economics), and a certificate in Entrepreneurship from Purdue University, West Lafayette, IN, USA, in 2023. He has received Dean's List honors for all completed semesters. He was the Vice President of Operations for the Habitat for Humanity campus chapter and the Treasurer of the Paint Crew basketball student section. He was an Electrical Engineer Intern with the Test and Automation Group, Milwaukee Tool in Summer 2021, then as an Engineering Intern in the Continuous Improvement Group, Kerry, in 2022. In 2022, he joined the Laboratory of Implantable Microsystems Research with the Weldon School of Biomedical Engineering, Purdue University. His research interests include the video analytics for Human Behavior Team at Purdue University and the Bio-Inspired Materials for Neural Interfacing Laboratory, Case Western Reserve University, Cleveland, OH, USA. His research interests include brain-computer interfaces and implantable medical devices.



Jongcheon Lim received the B.S. degree in materials science and engineering from Yonsei University, Seoul, South Korea, in 2015, the M.S. degree in bio and brain engineering from the Korea Advanced Institute of Science and Technology, Daejeon, South Korea, in 2017, and the Ph.D. degree in biomedical engineering from Purdue University, West Lafayette, IN, USA, in 2023. His research interests include implantable biosensors, microfabricated neural interface devices and soft implantable materials.



Chi Hwan Lee received the M.S. and Ph.D. degrees in mechanical engineering from Stanford University, Stanford, CA, USA, in 2009 and 2013, respectively. He is currently the Lesli A. Geddes Associate Professor of biomedical engineering and Associate Professor of mechanical engineering, and by Courtesy, of Materials Engineering, Purdue University, West Lafayette, IN, USA. Prior to joining Purdue in 2015, he was a Postdoctoral Research Associate with the Department of Materials Science and Engineering, University of Illinois at Urbana-Champaign, Champaign, IL, USA, under the guidance of Prof. John A. Rogers. His scholarly efforts are dedicated to addressing unmet clinical needs using novel yet simple wearable devices with a clear path towards translation to produce measurable clinical and economic impacts. He was the recipient of prestigious national and international awards including the 2021 Sensors Young Investigator Award, 2020 Purdue CoE Early Career Research Award, 2019 NIH Trailblazer Award, and 2019 Korean-American Scientists and Engineers Association (KSEA) Young Investigator Award.



Hyowon Lee (Member, IEEE) received the M.S. and Ph.D. degrees in biomedical engineering from the University of California, Los Angeles, Los Angeles, CA, USA, in 2008 and 2011, respectively. Before joining Purdue, he was a Senior Process Engineer for St. Jude Medical's Implantable Electronic Systems Division where he worked on implantable electronic devices such as pacemakers, implantable cardioverter defibrillators, deep brain stimulators, and spinal cord stimulators. At UCLA, he trained in the areas of neuroengineering and microfabrication under Jack Judy. His current research interests include centers around improving the reliability and functionality of implantable sensors and actuators for various medical conditions including opioid use disorder. He was the recipient of the NSF CAREER Award, and his lab is supported by NIH, NINDS, NIDA, NSF, Indiana CTSI, Samsung, and Eli Lilly.